Cold and Hot Slumped Glass Optics with interfacing ribs for high angular resolution x-ray telescopes

Civitani, M., Basso, S., Ghigo, M., Pareschi, G., Salmaso, B., et al.

M. Civitani, S. Basso, M. Ghigo, G. Pareschi, B. Salmaso, D. Spiga, G. Vecchi, R. Banham, E. Breuning, V. Burwitz, G. Hartner, B. Menz, "Cold and Hot Slumped Glass Optics with interfacing ribs for high angular resolution x-ray telescopes," Proc. SPIE 9905, Space Telescopes and Instrumentation 2016: Ultraviolet to Gamma Ray, 99056U (18 August 2016); doi: 10.1117/12.2232591

SPIE.

Event: SPIE Astronomical Telescopes + Instrumentation, 2016, Edinburgh, United Kingdom

Cold and Hot Slumped Glass Optics with interfacing ribs for high angular resolution X-ray telescopes

M. Civitani[a,1], S. Basso[a], M. Ghigo[a], G. Pareschi[a], B. Salmaso[a], D. Spiga[a], G. Vecchi[a], R. Banham[b], E.Breuning[c], V. Burwitz[c], G. D. Hartner[c], B. Menz[c]

[a]INAF Astronomical Observatory of Brera, Via E. Bianchi 46, I-23807 Merate (LC), Italy
[b]Media Lario Technologies s.p.a., 23842 Bosisio Parini (CO), Italy
[c]Max-Planck-Institüt für extraterrestrische Physik (Germany)

ABSTRACT

The Slumped Glass Optics technology, developed at INAF/OAB since a few years, is becoming a competitive solution for the realization of the future X-ray telescopes with a very large collecting area, e.g. the approved Athena, with more than 2 m^2 effective area at 1 keV and with a high angular resolution (5" HEW). The developed technique is based on modular elements, named X-ray Optical Units (XOUs), made of several layers of thin foils of glass, previously formed by direct hot slumping in cylindrical configuration and then stacked in a Wolter-I configuration, through interfacing ribs. The latest advancements in the production of thin glass substrates may allow a great simplification of this process, avoiding the pre-forming step via hot slumping. In fact, the strength and the flexibility of glass foils with thickness lower than 0.1 mm allow their bending up to very small radius of curvature without breaking. In this paper we provide an update of the project development, reporting on the last results achieved. In particular, we present the results obtained on several prototypes that have been assembled with different integration approaches.

Keywords: X-ray grazing-incidence telescopes, replication techniques, X-ray segmented mirrors, cold slumping, hot slumping of glass foils, integration and alignment

1 Introduction

During the last years, the realization of X-ray Optical Units (XOU) for future large size X-ray telescopes, based on the segmented configuration, is being investigated with different technologies. The "Pore Optics" technology, in which a module is formed stacking special-wedged silicon wafers, is pursued in Europe by ESA [1,2]. In USA, NASA-GSFC has investigated the utilization of thermally shaped thin glass foils. Now, the technique evolved toward the use of direct polished Silicon wafers [3].
The Slumped Glass Optics (SGO), developed at INAF/OAB since some years, is an effective option to realize future X-ray telescopes [4]. This technology is based on the use of thin glass plates that can be procured at low cost with high quality surface micro-roughness. Depending on the size of the mirror assembly, a complete mirror module or single X-ray Optical Units (azimuthal and radial segments of the final optical module) can be made as assemblies of segmented glass plates. The plates, flat or pre-shaped to a cylindrical profile by direct hot-slumping, are figured to the final Wolter-I configuration through the integration process. It operates with the cold slumping approach by means of integration molds with parabolic and hyperbolic shapes [5]. The integration process, operated trough a dedicated Integration Machine (IMA) [6], also enables the correct relative alignment of the plates within each tandem and for the entire stack.
As a follow-up of the activities started in the context of the IXO project [7], a mechanical design of the overall mirror module based on the glass technology has been studied in collaboration with MPE for an "ATHENA-like" concept mission (focal length 12 m, radii 220-1000 mm) [8]. The hot-slumping and integration activities, indeed started in 2009 within an ESA contract, continued during the years with improving results [9, 10]. Nevertheless, it has been recently argued that the glass technology can be pushed forward reducing the thickness of the plates down to 50-200 microns: in this case, the initial pre-shaping in cylindrical configuration can be avoided reducing the cost production and preserving completely the micro-roughness of the glass surface. This new process [11] has been patented and has been studied for a medium size mission (focal length 10 m, radius 220-480 mm) [12].

[1] Corresponding author: marta.civitani@brera.inaf.it;; www.brera.inaf.it

Space Telescopes and Instrumentation 2016: Ultraviolet to Gamma Ray, edited by Jan-Willem A. den Herder, Tadayuki Takahashi, Marshall Bautz, Proc. of SPIE Vol. 9905, 99056U
 · doi: 10.1117/12.2232591

In this paper we present an overview of present integration options and the recent improvements of the integration process. Moreover, the latest results achieved with the integration of hot and cold slumped glass substrates are presented together with the x-ray calibration data. In the end we present the plan for the future activities.

2 Overview of the integration possibilities

The integration activity, based on hot slumped glass, started in 2011. It initially followed the IXO optical design prescriptions, with a focal length of 20 m. The radius of curvature of the developed segments was 1 m, representing an average value throughout the series of shells to be developed for the mission. Due to the long focal length, it was necessary to develop a dedicated set-up for the x-ray calibration at Panter/MPE facility [13]. More recently, we started exploring different optical configurations. In this respect, the major operational constraint is the availability of the integration molds to be used for the integration. In the following it is reported the list of the explored optical configurations at our group, discussing the problematic related to each set-up.

- **20 m focal length and 1 m radius of curvature**. Two sets of integration molds with a focal length of 20 m and a radius of curvature of 1m were procured in the framework of the ESA contract. The first is made of Metapore, while the second is made of BK7. In all the cases, the optical area is optimized on the size of the slumped glass, 200 mm x 200 mm for both the parabolic and the hyperbolic segments. There is a gap of 20mm along the optical axis between the two optical areas. The Metapore is a composite porous material, suitable for vacuum suction, but difficult to figure with high accuracy. Moreover, due to its aluminium content, its Coefficient of Thermal Expansion (CTE) is rather high and not ideal for matching the CTE of glass during the integration. This first mold tandem has been used for the realization of the very first two prototypes developed by our group. The Proof of Concept #1 (PoC#1), realized in late 2011 and the XOU_BB (acronym for "X-ray Optical Unit Breadboard"), assembled in 2012 in a representative mechanical configuration, including a frame in titanium representing the interface with the satellite structure [14]. As the figure error of the integrated glasses was mainly related to the integration mold, a second set of integration molds with the same optical configuration have been procured: the BK7 molds were figured at Zeeko Ltd to a final HEW of around 3-4" each. A new proof of concept (PoC#2) has been realized in early 2013 (figure 1C) by means of these new integration moulds and new AF32 glass slumped on Zerodur mold, with better optical quality with respect to the previous segments. It was based on 4 Pair Plate (PP) layers (1 dummy pair + 3 optically representative pairs). Moreover, the layers were mounted in co-focal configuration, in order to check the alignment performance of the IMA. The achieved results showed a relevant step forward achieving an HEW of 22.1" in full illumination mode @0.27keV [15]. This BK7 integration tandem has been used in the following years to fabricate other prototypes based on direct hot slumped glass [15, 10], but, for different reasons, the PoC#2 remain the best result achieved so far. The results, related to the last prototype (PoC#5) integrated beginning of 2016, are presented in paragraph 4.

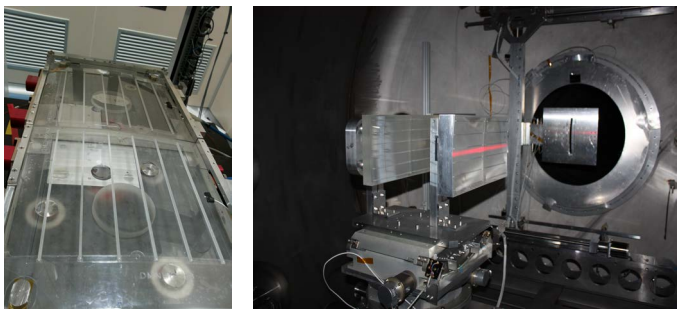

Figure 1: Measurement configuration @Panter/MPE for the PoC#5d and the WP1, measured end of June 2016. The two prototypes are supported independently on the same flange so that they can be measured one after the other without interrupting the vacuum chamber configuration.

Furthermore, these integration molds have been used to realize the first integration tests based on a full cold slumping approach of Willow glass plates with 200 microns thickness. The WP0 has been realized in 2015 while the WP1 and the WP2 have been integrated in 2016. While the metrological results and the x-ray calibration output of WP1 are reported in paragraph 5, the metrological characterization of WP2 is not complete yet and the data will be presented in the future.

These molds are still available but all the mechanical interfaces to the IMA have been dismounted and recycled on the BK7 tandem. Recently, some of the interface items have been dismounted from the BK7 tandem of integration molds, in order to allow imparting a refinement of the profile errors via ion beam figuring. Only when this activity is completed, they will be re-installed and the 3D alignment process repeated to restore their full functionality. In the meantime they can be used only for integration tests, careless of the relative alignment, but useful to validate the integration model.

- **7.4 m focal length and 0.5 m radius of curvature**. This is a monolithic (Parabola + Hyperbola) mold, dedicated to the integration of indirect slumped glass produced within an internal effort at MPE [16]. The mold is made of Aluminium and precisely machined by the LT-Ultra GmbH company. Due to its monolithic configuration, there is no need for interfaces versus the autocollimator chain to enable their mutual alignment. Only a mechanical interface is used to fit the supporting structure and to interface it with the linear encoder system. Unlike the other molds, the optical area in this case is smaller, being 100 mm x 100 mm for parabolic and hyperbolic segments. The activities related to the integration of the indirect slumped glasses from MPE are at this moment in stand-by, waiting for an improvement in the glass segments quality (produced via thermal slumping). Due to the particular geometrical configuration, its use for the cold slumping replica could be foreseen only with a dedicated optimization of the ribs pattern.

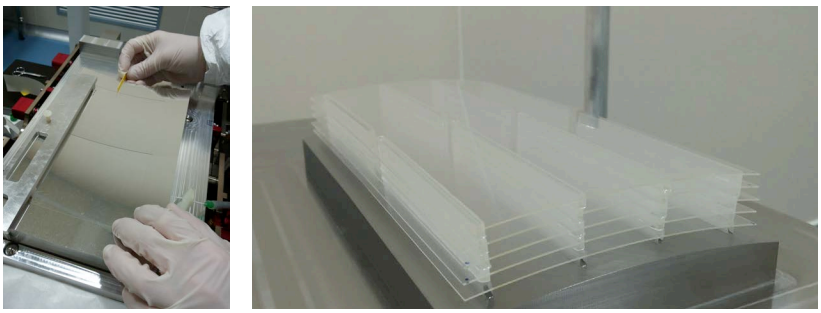

Figure 2: (A) Monolithic concave mold dedicated to the integration of indirect slumped glass provided by MPE. (B) JIM prototype made in 2015 with 5 glass layers.

- **8.4 m focal length and 0.485 m radius of curvature**. The integration mold tandem, made of aluminium has been procured from LT-Ultra GmbH to allow to integrate the slumped glass produced by NASA [17]. The optical area is around 127 mm x 200 mm for both parabolic and hyperbolic sections, with a gap of about 50 mm at the intersection plane between the two (see figure 3A). A first module, based on hot-slumped glass, has been produced but its metrological characterization is not yet concluded yet at the time being (figure 3B). Due to its optical configuration, this integration tandem allows the fabrication of module compatible with the standard (no extension) Panter/MPE set-up. It will be used for both hot and cold slumping integration experiments.

Figure 3: (A) the integration mold tandem for the 8.4 m focal length. The corresponding radius of curvature @IP is 485 mm. (B) The first integration trial based on the glass slumped by NASA.

- **12 m focal length and 1m radius of curvature.** These integration molds are made of Fused Silica. They have been obtained grinding in Wolter-I configuration old cylindrical slumping molds. They will be polished with the IRP1200 Zeeko machine and figured with the ion beam facilities in INAF/OAB laboratories.

3 Integration process up-grading

Different activities have been done and are currently on going to up-grade the technology and to acquire a better comprehension of the process. They are reported in the next paragraphs.

3.1 Dust particle detection process at work

The quality of the cold slumping replica is related to different variables, like the rigidity of the structure, the fixture pattern and the bonding shrinkage. Above all, it is fundamental that the surface of the thin sheet replicates as much as possible the surface of the reference. Our process is performed in a clean room environment (ISO6) but the level of cleaning is not sufficient yet for our purposes. We have experienced that the entrapping of dust grains between the two surfaces is a major operational problem as it prevents the thin sheet from perfectly replicating the shape of the integration mold. In this condition the replica cannot be perfect.

Normally, the glass plate positioning on the integration mold is repeated under airflow as many times as needed with a feedback to evaluate the amount of dust present until the desired level of cleanliness is achieved. A dust particle detection system has been implemented on the IMA, in order to trace the position and the amount of glass distortion during this preparatory phase. It is based on the deflectometry technique used in differential mode. Comparing the image of the reflected pattern from the reference mandrel surface with the reflected pattern recorded after the thin sheet positioning, the bumps of the dust grain are easily highlighted. In this way the dust presence appears in the measurement as a higher frequency slope error variation in correspondence of the dust grain [10]. This type of measurement is extremely versatile as can be adapted to the shape of any reference mold. A null-configuration measurement of the mandrel is taken before starting the actual final measurement series. Thanks to this differential concept, the system intrinsically enables the characterization of free-form optics and using multiple cameras it is also possible to map any kind of mirror shapes. Furthermore, as anticipated, it overcomes all problems due to the systematic errors caused by the alignment of the different parts and it works for uncoated and coated glass substrates.

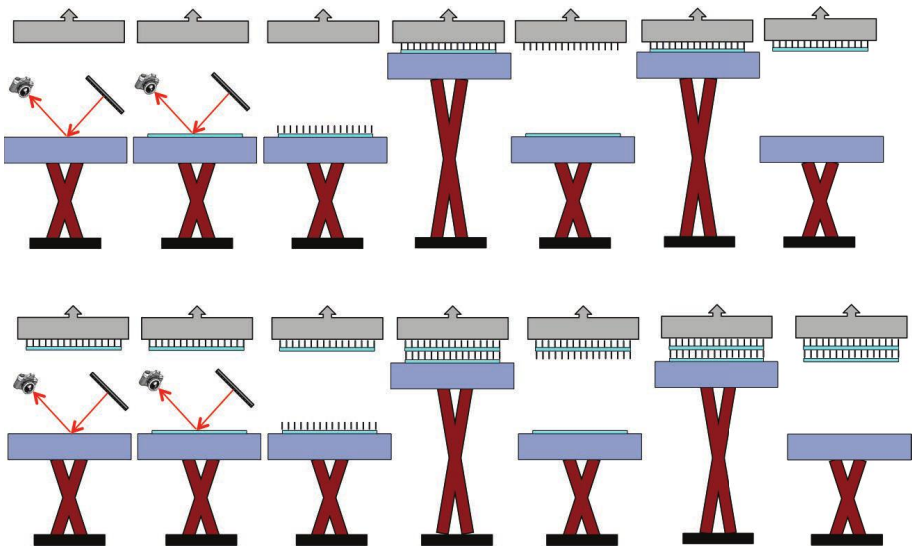

Figure 4: The integration steps with the dust particle detection system.

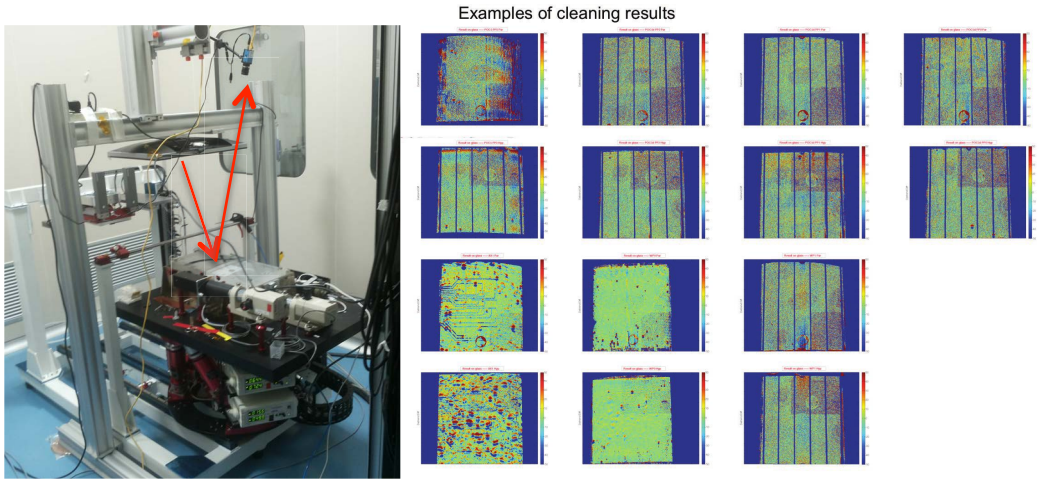

Figure 5: Dust particle detection set-up implemented on the IMA based on the deflectometric approach. (A) The hardware on the IMA. (B) Some of the output results achieved during the integration process.

The process steps are reported in figure 4. A reference measurement is taken on the mould surface before positioning the plate to be integrated. The measurement is repeated when the plate is on the mould and the vacuum suction is applied. The difference between the two slope maps returns the locations of the dust grain entrapped. If the cleanliness condition is judged sufficient, the integration procedure continues, otherwise the cleaning procedure is repeated up to the desired condition. For each of integrated plates, we have now a recorded trace of the reached level of cleaning and the integrated glass plate shape can be correlated with the initial mismatch between the reference mandrel and the thin plate (see paragraph 4.2) The implemented set-up is showed in figure 5. The system is currently in use since some months: examples of the system output recorded during different modules integration are reported in figure 5B. The system has been very useful to verify that a change in the optical paper quality was a major improvement during the set-up of the glass.

3.2 Glue distribution system up-grade

During the years, the glue distribution has been recognized as a critical part of the integration procedure. It was performed by means of a dispenser, controlling two syringes to be manually aligned with the ribs and the glass. The relative distance, the alignment and the pressure of the dispenser concur to the lack of repeatability in terms of the amount of glue and spatial distribution. Moreover, due to the mechanical set-up, in most of the cases the edges of the ribs were not completely bonded. As this is a critical condition for the cold slumping approach, the glue distribution system has been modified.

A completely different scheme has been then introduced adopting a cost-effective glue-printing procedure. A wire keeps the glue up to the transfer of the rib surface. The alignment between the wire and the ribs is much more easy than the one with syringes and the glue can completely cover the ribs on the top and the bottom edges. The amount of glue to be printed is function of the wire section and can be verified during the process on a different surface. With this new procedure, the glue can be printed directly on the ribs also during the glass-bonding phase avoiding possible misalignments between the ribs already bonded and the distributed glue on the glass. In Figure 6, the tool and the set-up are shown, while the glue distribution procedure on the ribs is reported in Figure 7.

The procedure has been developed and optimized during the integration of the PoC#5 module. Metallic wires with different thickness have been tested in order to get the right amount of glue. Nevertheless, synthetic wires, which have been verified to be the best solution, have been used only after the PoC#5d production. Metallic wires tend to introduce glue dots that can be smoothed out via little movements of the wires. On the other hand, the glue deposited with synthetic wire appears smooth from the beginning. The procedure is still under optimization and different wire thicknesses have been procured and will be tested to determine the most effective.

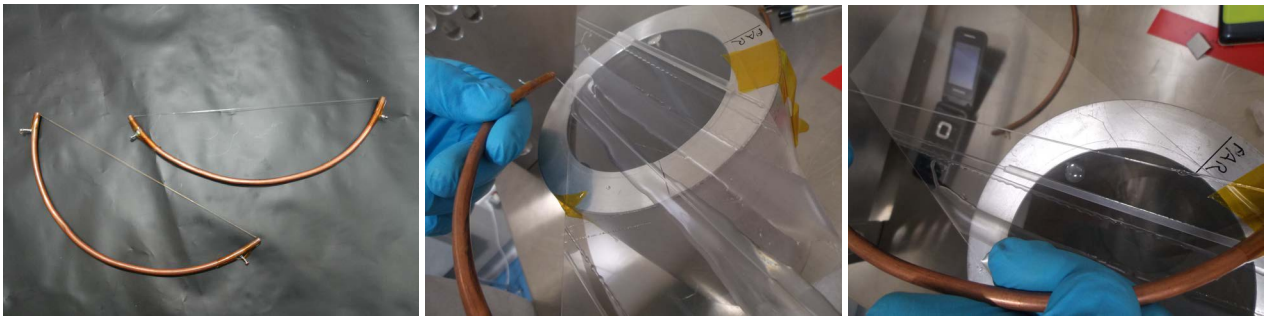

Figure 6: New Glue distribution process: a nylon wire is immersed in the glue and then used to stamp the glue. The amount of glue is function of the diameter of the wire.

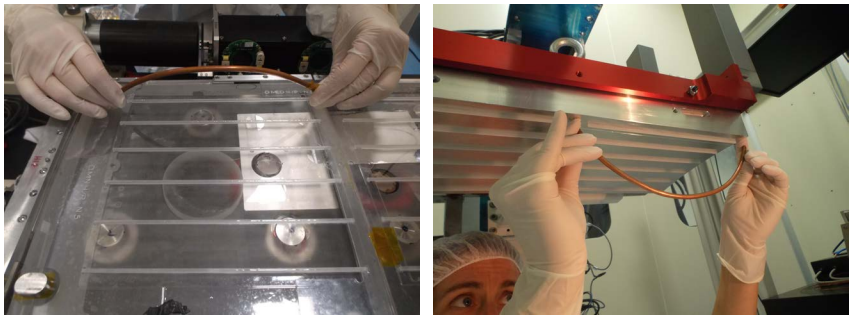

Figure 7: The glue is printed directly all along each rib in both the ribs interface bonding integration steps.

The advantages of the new system are hereafter summarized:

- the glue is always distributed along the ribs so that the direction of the glue line is correct;
- the ribs surface is rough and the glue remains in position and does not flow on the glass due to the radial curvature;
- the control on the amount of the glue is higher;
- the distribution all along the rib can be controlled (no dots);
- the edges of the ribs are fully bonded;
- the glue distribution is possible also in case of small radii of curvature.

3.3 On going activities for IMA on-board metrology

In the present IMA configuration, while the stack is growing under the backplane, there is no feedback on the integration result. Only when the stack is completed and dismounted, the metrology on the lastly integrated PP is possible. However, this operation may introduce a high degree of uncertainty on the final expected results. In order to overcome this problem, a second deflectometric equipment is under installation on the IMA. This is based on the same working principle of the one realized at MPE for the Alignement Machine [18]. In the current set-up, two cameras are installed and dedicated to the metrology of the parabolic and the hyperbolic segments. The conceptual design and the hardware configuration are presented in figure 8A and figure 8B. The procedure steps are illustrated in Figure 9. After the bonding of each plate, a reference measurement will be taken. Once a new set of ribs is glued onto the plate, a new measurement is provided and can be compared with the previous one. This comparison will allow us to determine if/how the plate is deformed by the ribs bonding. Moreover, each of the bonded layers will have a correspondent error map to be compared with UV/X-ray data.

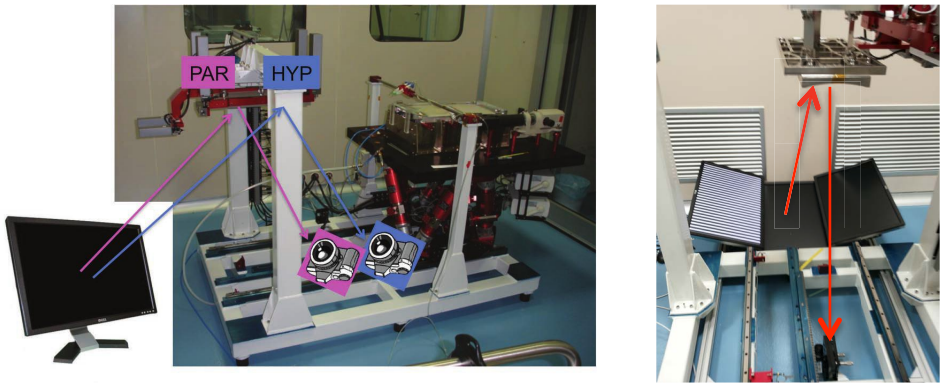

Figure 8: The IMA on board metrology system. (A) The metrology concept. (B) The hardware on the IMA.

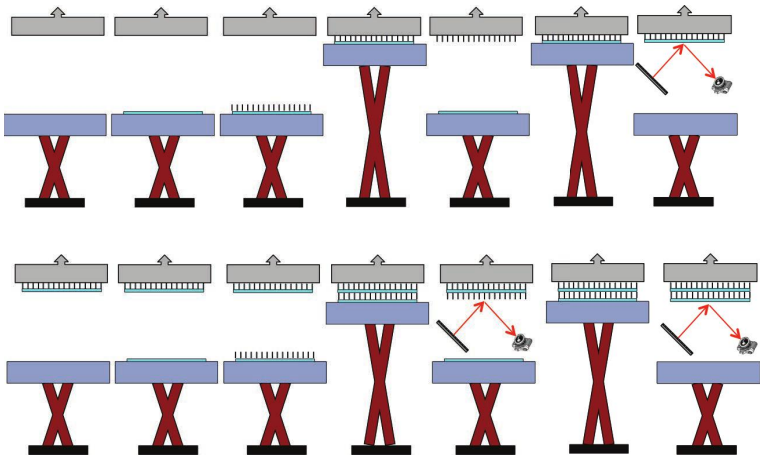

Figure 9: The integration steps with the deflectometric measurement system.

4 Integration of Hot slumped Glasses: PoC#5 results and analysis

The PoC#5, made at the beginning of 2016, is composed as usual by 4 layers of slumped glasses assembled in co-focal configuration. It has been realized with the BK7 integrations moulds: the focal length and the radius of curvature at the intersection plane are respectively 20 m and 1 m. The optical configuration is the same used for the PoC#2 and PoC#4. Unlike PoC#4, in this case all the four layers are made of non-coated Eagle hot-slumped glasses. Due to the limited number of available plates, it has been decided to maintain this simplification in the system and to postpone the integration of coated glasses in the tests dedicated to cold slumping approach, which guarantees much more flexibility.

4.1 Metrological characterization before integration and expected performances

Before the integration, the metrological characterization of the glass figure errors has been realized with different instruments. The mono-dimensional error data acquired with the Long Trace Profilometer (LTP) instrument are presented in another paper from our group [9]. In order to provide a complete 3D map of the glass figure error, the CUP metrology system [19] has been used. In figure 10A we show the residuals with respect to a theoretical cylinder with radius of curvature of 1 m, which is used as reference in all FEM simulations. Depending on the slumping process, the radius of curvature of the slumped glass is different. The PtV of the residual azimuthal error ranges between 90 and 150 microns. These variations correspond to best-fit radius of curvature ranging between 971 and 983 mm. Depending on their azimuthal position, the longitudinal profiles have a different shape and amplitude. The relevant data in terms of PtV and RMS for each of the acquired profiles is reported in figure 10B. In general, the central part appears better than the lateral parts and there are two

symmetric positions, at about -70 and 70 mm in which the residual errors are smaller. In figure 11A the typical residuals are shown (after having evaluated the cylindrical best-fit). The residual shape presents twists of several microns on the edges, so that the longitudinal profiles are not all on the same plane. The accurate measurement of this kind of features is not possible in the present CUP set-up due to limited accuracy of the carriages. Some artefacts (jumps and steps) are introduced randomly in the measurements. They can be partially recovered by software correction but they prevent the complete and accurate characterization of the glass foils.

Until now, a simplified description of the glass figure errors has been adopted. Following the results provided in [5], a complete correction of the azimuthal error and a partial (e.g. wavelength dependent) correction for the longitudinal profiles have been assumed. The two components are treated independently. As the ratio between the radius of the integration mandrel and the slumped mirror segments is below 1.1 (in these cases is reaches 1.031), the contribution to the HEW should be less than 2". Moreover, the misalignment between the longitudinal profiles has been neglected and low frequency errors are supposed to be fairly corrected by the integration process. Hence, the expected results have been retrieved assuming a simplified configuration with minimum misalignment (Fig. 11B), and by means of a corrective matrix (Fig. 11C) they have been damped according to the wavelength error in Fourier space. The expected overall error after the damping process is shown in top panel of figure 11D, while the inferred HEW, before and after the dumping factor application, is reported in the bottom panel, in correspondence to each longitudinal profile.

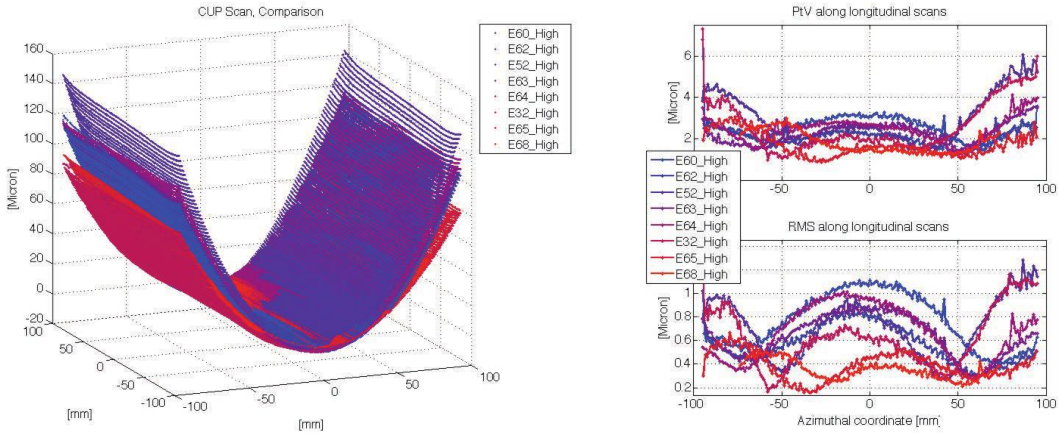

Figure 10: (A) Overall residua with respect to a cylinder with a radius of curvature of 1m. (B) Longitudinal profiles PtV and RMS in dependence of the azimuthal position. (C) Example of the residuals with respect to the best-fit cylinder for one of the glass.

In order to provide a better characterization of the process and to verify if the simplified model is reliable, FEM simulations have been carried out starting from the CUP measured data. In figure 9 is reported, as an example, the FEM simulation results corresponding to the same glass used in figure 8 to illustrate the damping process results. In figure 9A is reported the expected residual map after the integration with the same colour scale of figure 8D. It is evident that the expectations for the two models are not comparable: in the FEM model the amplitude of the residual low frequency errors is higher. In figure 9B the mean PSD of the longitudinal profiles (initial, simplified dumping model and FEM model) are reported. The correspondence between the initial data (black) and the simplified model for damping the data (green) ends at around 20 mm where the integration corrective capability starts to act. As the data provided for FEM simulations have been filtered at higher frequencies to avoid convergence problems, the corresponding PSD in lower in this range. At greater wavelength it remains higher than the one calculated with the simplified model. The comparison between the PSD shows clearly that for higher wavelength the damping efficiency is lower than for the simplified model. This translates in expected HEW results as reported in figure 9C. In green and in blue the results from the simplified dumping and the FEM simulations are reported. Due to the low frequency errors remaining in the integrated glass, the HEW calculated from the FEM data is worse in the central part.

The analysis and the optimization of the FEM simulations are still on going. At the moment, due to systematic errors and to the noise in the measurement data it is not always possible to have a reliable feedback for all the glasses.

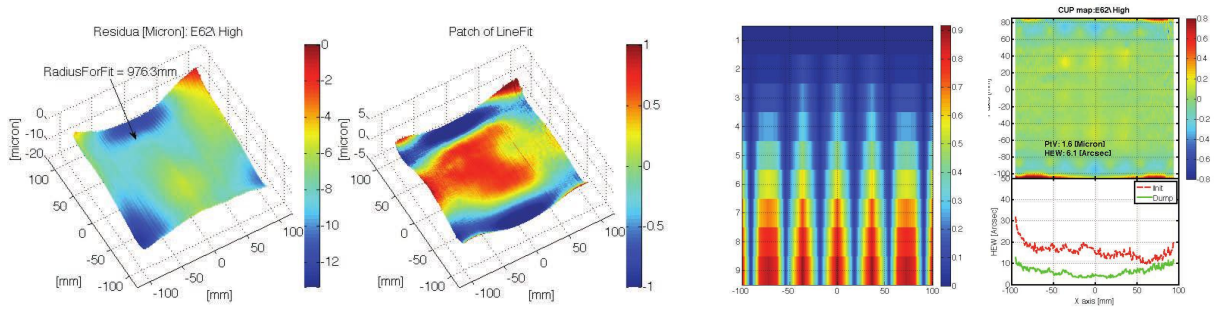

Figure 11: (A) Overall residuals with respect to the theoretical reference cylinder of 1m radius of curvature. (B) The simplified-model starting map assumes only longitudinal profile errors, neglecting azimuthal residual curvature and tilts. (C) The corrective damping map to be applied in Fourier space: according to the wavelength and to the relative position with respect to the rib, the corrective factors can be more or less effective. (D) The damped maps according to the simplified model and the corresponding results.

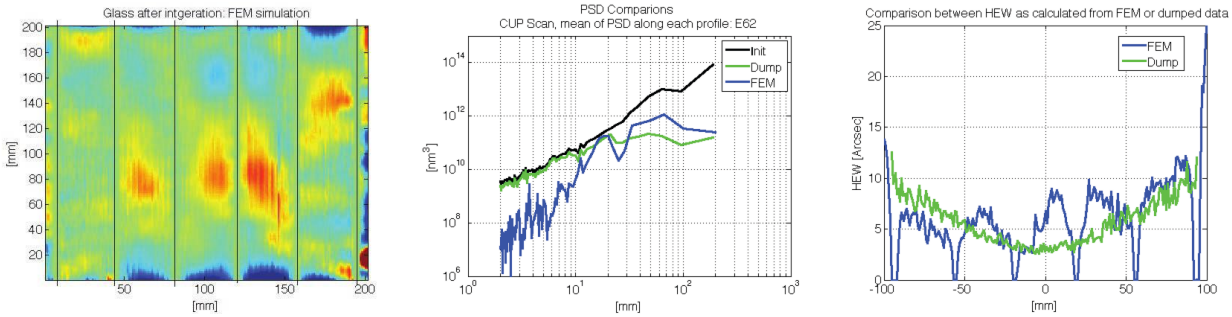

Figure 12: (A) Residual error results on the integrated glass as derived from FEM simulations (glass E62). (B) The mean PSD of the longitudinal profiles: as slumped (black), after the integration assuming the simplified dumping factor model (green) and after the integration assuming the complete FEM model (cyan). (C) The expected HEW on the different longitudinal profiles estimated with the two approaches.

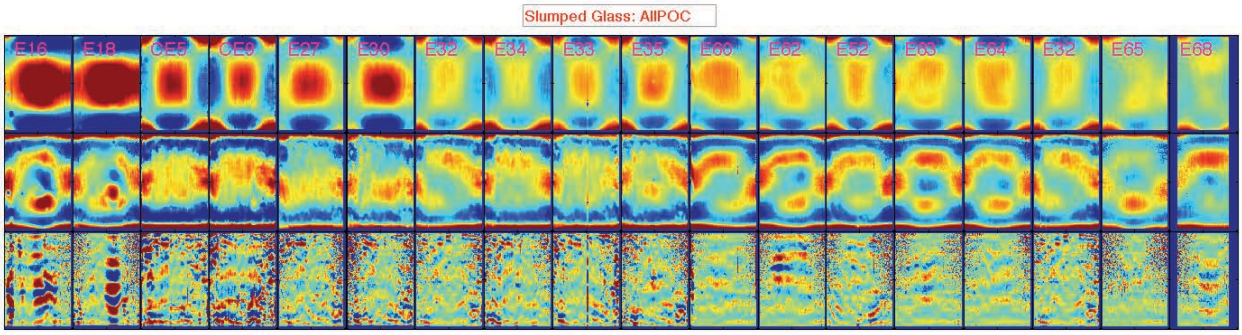

Figure 13: The slumped glass metrology before integration of the last PoCs. E16 and E18 have been integrated in the PoC3. From CE5 to E35, the segments have been used for the PoC#4. From R60 to E68, the glass have been integrated in the PoC5d.

In figure 13 we compare the figure error of the glasses integrated in the last prototypes. Each column refers to a glass sample, while in the three rows the longitudinal profiles are shown after the removal of average value and tilt, the second and then the 8th order Legendre polynomials to evidence the presence of higher frequency errors. E16 and E18 composed the PoC#3, while CE5 and CE9 were the coated glass integrated in the PoC#4, together with E27, E30, E32, E34, E33 and E35. The glasses after E60 were integrated in PoC#5d. As the colour scale is constant in each line, it is immediate to notice the reduction of the low frequency error amplitude and the reduction on the edge of the mid-frequencies content. In

general, the expected HEW for all the glasses that compose the PoC#5d, estimated from the simplified model, is around 8": central parts of the glass are around 5" while the HEW increases to around 10" on the sides.

4.2 Metrological characterization after integration

Due to some operational problem, the integration of the last developed prototype (PoC#5) has been restarted a few times. In this way we had the opportunity to test the integration procedure and the related performance. The first attempt for the module integration has been aborted after the bonding of the first layer (PoC#5a). The glue was been distributed with the previous method, i.e. by mean of dispensers (syringes). Moreover, a too large amount of glue was used, so that the dispensed glued was overflowing on both of the sides of all the ribs. The thickness was set to 100 microns. The results achieved on the integrated glass can be compared with the one obtained on the final integrated prototype (PoC#5d). In this last case, the glue distribution system was already changed and 50 microns of glue were constrained better on the ribs sections.

After dismounting the layers of the stack assembled during the different attempt, the external layer of the different proof-of-concepts has been measured with the CUP metrology system. The residuals with respect to the theoretical Wolter-I shape (Parabolic and Hyperbolic) are reported in figure 14 and in figure 15. In the first column is reported the shape of the figure error of the integration mold, while in the following we show the results for the PoC#2, PoC#3, PoC#4, PoC#5a and PoC#5d. As in the previous figure the first line show the longitudinal profile errors while in the second and the third are reported the residua after the removal of the second and the 8th Legendre polynomial. Each row has the same color scale.
The amplitude of the low frequency error is progressively decreasing. The remaining mid-frequency errors are partially due to the initial quality of the integrated glass (see Figure 13 for glasses that compose PoC#3, PoC#4, PoC#5a and PoC#5d) and partially due to the local deformations introduced by the dust grain entrapped under the glass during the integration procedure. In Figure 16 are reported the deflectometric maps acquired during the glass-positioning phase of PoC#5d. These data have to be compared with the results in Figure 14 and Figure 15 (last columns). The correspondence between the recorded dust grains in correspondence to the ribs locations and the local deformation with higher amplitude visible at the ribs locations is impressive and gives us a immediate feedback of the cleanliness requirement. As the level of cleanliness of the other layers of the PoC#5d was almost comparable with the one of PP0, the same kind of features are expected to characterize all the integrated glasses. In order to better control the quality of the integrated glasses, we need to further improve the cleanliness level.

Comparing the results achieved on PoC#5a and PoC#5d, it is clear that, by chance, the effect of the entrapped dust grain is higher on the PoC#5d parabolic section with respect to the PoC#5a, while the situation is opposite on hyperbolic sections. Nevertheless, in absence of major local deformations in correspondence of the ribs, the glass surface shows limited amount of mid-frequency errors (PoC#5a Parabola and PoC#5d Hyperbola) with respect to the older PoCs.

The different glue distribution performances do not seem to have a huge impact on the integrated glass geometry (at least for the first integrated layer): parabolic sections of PoC#5a and PoC#5d are almost similar, despite to the effects of dust grain entrapped under the ribs. The similarity is lower for the hyperbolic sections. Due to the differences of the initial shape of the integrated glass and to the unclear effect of the dust grain entrapped in the portions of glass between the ribs, the similarity of the results achieved with two completely different glue distribution performances cannot be conclusive. This is clearly an interesting aspect and further tests will be carried out in the future. In particular, since the metrological characterization of the external layer of the PoC#5d is not in line with the results obtained during x-ray calibration (see paragraph 4.3), it should be also verified that the long term curing of the glue did not change the shape of the integrated glass.

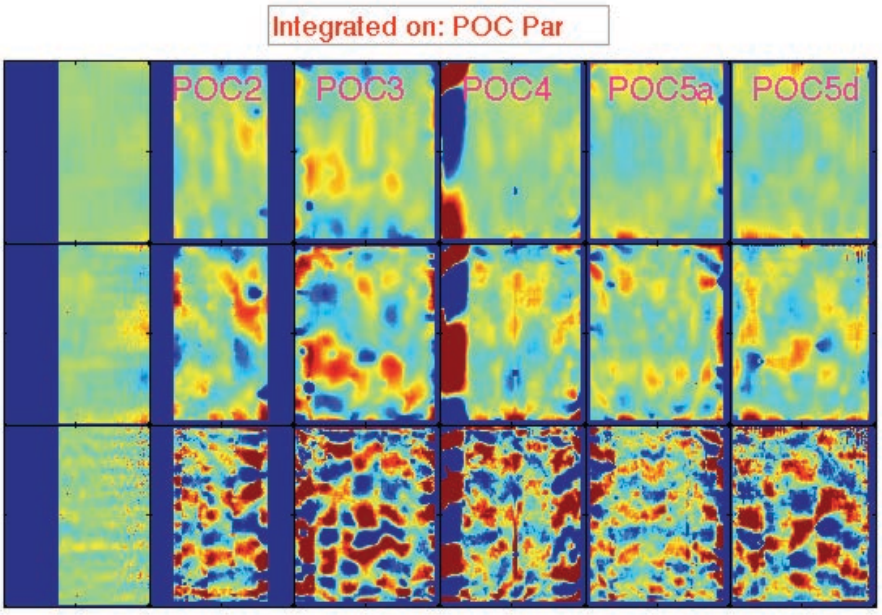

Figure 14: The figure error of the external layer (parabolic segments) of the different PoCs (POC2, POC3, POC4, POC5a and POC5d) integrated in the last years compares with the available data of the integration molds (first column). Top row panels show the longitudinal profiles errors, the middle row represents the profile errors after the removal of a second order Legendre polynomial and the bottom row panels report the profile errors after the removal up to the 8th order Legendre polynomials.

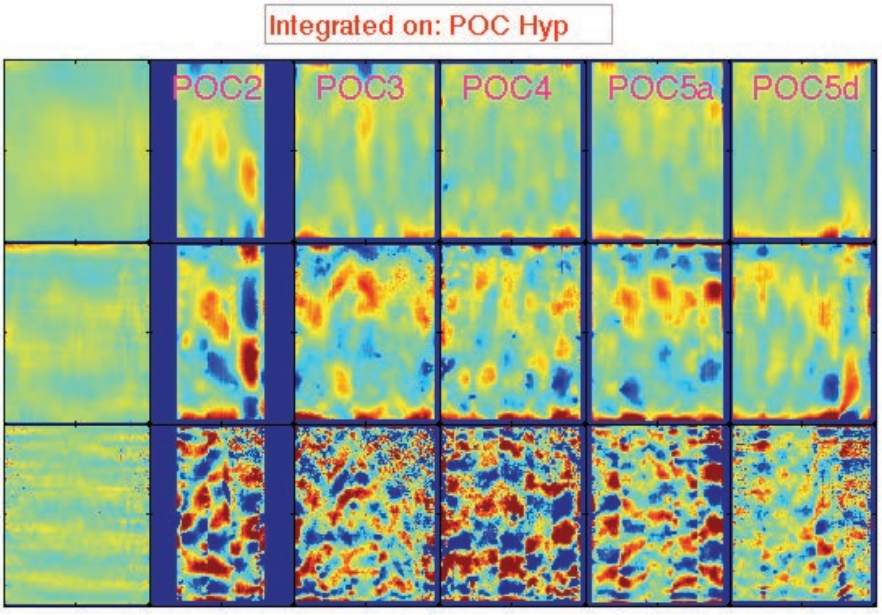

Figure 15: The figure error of the external layer (hyperbolic segments) of the different PoCs (POC2, POC3, POC4, POC5a and POC5d) integrated in the last years compared with the available data of the integration molds (first column). Top row panels show the longitudinal profiles errors, the middle row represents the profile errors after the removal of a second order Legendre polynomial and the bottom row panels report the profile errors after the removal up to the 8th order Legendre polynomials.

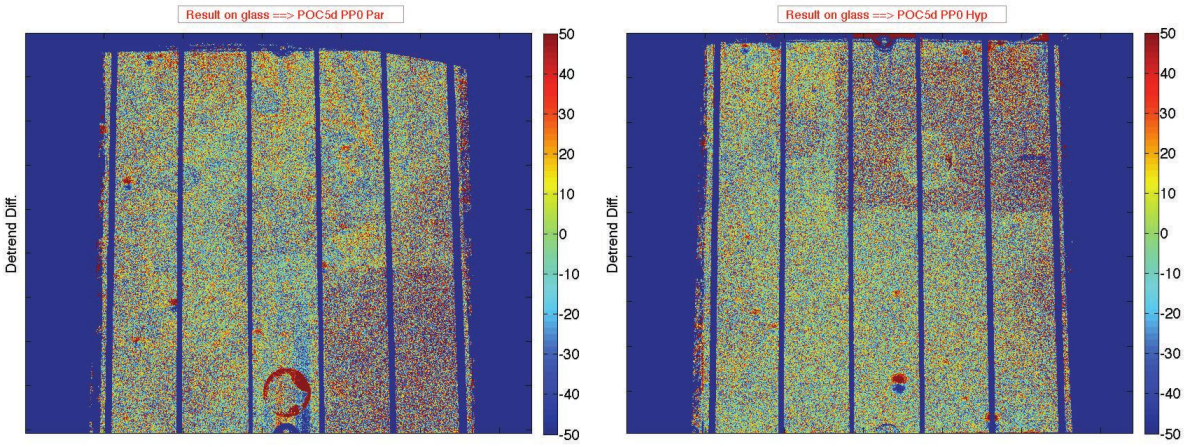

Figure 16: The output of the dust particle detection system on board the IMA for the glasses integrated as PoC5d PP0 layer. The dust grain detected in the ribs regions corresponds clearly to measured effect on the integrated glass maps (figure 14 and figure 15).

In order to highlight the differences with respect to the previous integrated modules, the results for different PoCs are presented in Figure 17 in single reflections for parabolic and hyperbolic sections. The overall performance of PoC#5d shows an improvement of the quality of the integrated glass (except in correspondence to local deformations). Unfortunately, these metrological results have not been confirmed by the x-ray calibration data, performed end of June 2016 (see paragraph 4.3). The overall HEW for the PP0 is higher (around 30") and also the pencil beams scan shows a completely different behaviour. As a positive crosscheck with the metrology was already been carried out in the past [2014, 2015], this result was really unexpected. In particular, for the PoC#4, the expected HEW from the ray-tracing simulations in double reflection was around 14": this result was comparable with the measured values (in the region of the glass far from the ribs) at Panter in the pencil beam scan. As the PoC#5d is on average slightly better than the PoC#4, a dedicated test campaign on the module will be carried out as soon as the module returns to our labs to verify if something happened to the layers.

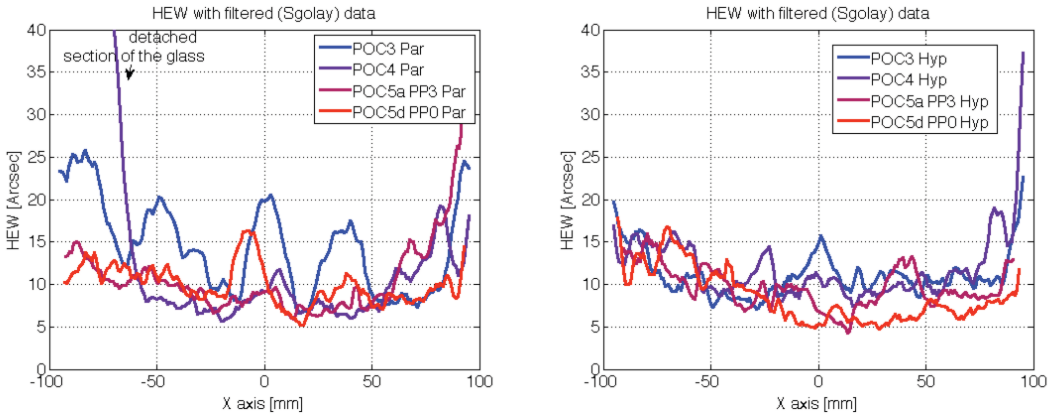

Figure 17: Comparison between the HEW as derived from CUP maps as acquired on external layer of PoC#3, PoC#4, PoC#5a and PoC#5d. Results achieved on the parabola and on the hyperbola are reported on the left and on the right panel respectively.

4.3 X-ray calibration: in focus measurement

As previously anticipated, the x-ray calibration at the Panter/MPE x-ray facility [13] of the PoC#5d has been performed in the same calibration sessions of the WP1. The two modules were mounted in an almost parallel configuration and measured one after the other. In Figure 1B it is reported the set-up adopted for the manipulator in the vacuum chamber. The alignment of the module has been retrieved with PIXI data, optimizing the flux (of the whole module) with respect to the different rotation directions [20]. The results presented in the following are all acquired at an x-ray energy of 1.49 keV, as it corresponds to the optimal signal to noise ratio in the current set-up.

A mask was developed to isolate the different PP components. This mask has been used in combination with a diagonal mask to provide a pencil beam set-up. The pencil beam scan of the PoC#4 [10] showed that in correspondence to the ribs the HEW was higher and the bonding quality was one of the possible causes. A dashed and a complementary mask have been realized to quickly evaluate the HEW in correspondence of the ribs and of the portion of the glass between the ribs. Due to the limited amount of time available for the entire test, the mask provided a quick feedback on the quality of the bonding, avoiding the complete pencil beam scan of each plate. The results achieved for each of the PP are reported in Figure 18A. The HEW of the glass region near the ribs is reported in pink while the HEW of the other part of the glass is in yellow. The region near the ribs is better than the remaining part of the glass. This is true for all the PPs. The value measured near the ribs is around 25", i.e. a much lower level than the ones measured in the same way in the past, which was around 35" [10]. Moreover, it should be noted that the portions of the glass between the ribs dominate the overall HEW of the glass. The corresponding values, acquired with the standard long slit, are reported as black stars in the graph. This result is due to the improvement in the glue distribution system.

As anticipated, despite this encouraging result, the optical performances of the different PP are not better than the one acquired on the previous prototypes. In Figure 18B, it is reported the HEW of each PP: it is compared with the corresponding result achieved on previous prototypes (if available). All the data are given at 1.49 keV. The HEW for all the PPs remains around 30" and it is almost comparable with the one achieved with previous prototypes: the average HEW is not decreased.

Unlike previous tests, in the PoC#5d the best layer is the innermost and not the external one. This is a positive indication for the optimization of the process. When the innermost layers are worst than the outer, a cumulative integration error can be supposed and this can degrade the performances of the complete assembled system. In the PoC#5d, for the first time, the trend is reversed with the better layers being the first integrated. Further analysis on the effect of the integration on the already integrated layers will be possible when the deflectometric measurement system is operative on the IMA.

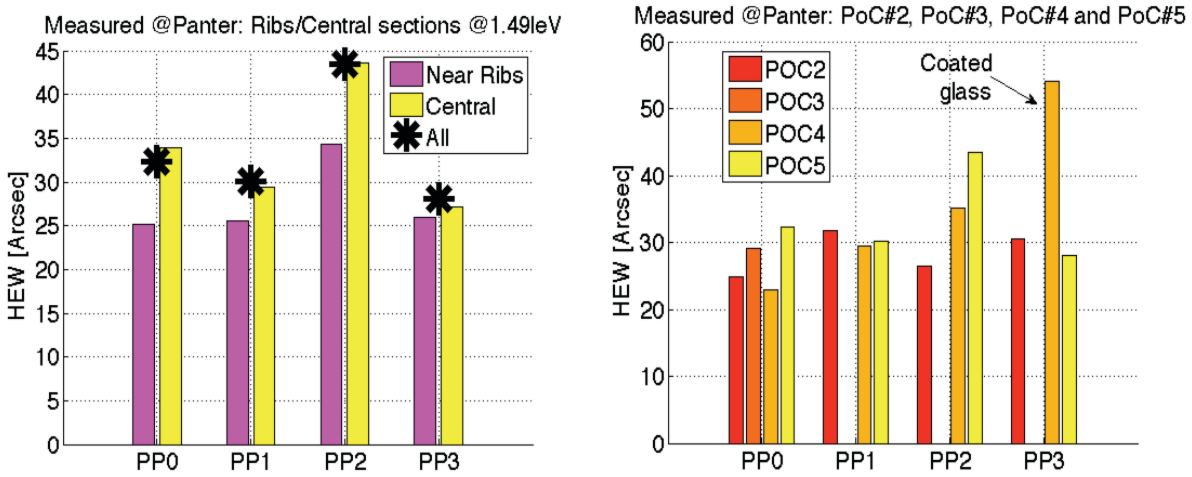

Figure 18: (A) HEW of the different layers of the POC#5d with a dashed and an complementary mask: the HEW is evaluated in correspondence of the ribs (magenta) and of the portion of the glass between the ribs (yellow). In black the HEW of the complete PP. (B) The HEW of each PP at its best focus. Colours (from red to yellow) refer to the different prototypes (PoC#2, PoC#3, PoC#4 and PoC#5d). The PoC#4 PP3 was a dummy layer integrated for test the integration procedure with coated glasses.

4.4 X-ray calibration: pencil beam scans

The pencil beam procedure developed at Panter/MPE on the JIM module [16] had to be adapted to the layers of PoC#5d. Instead of having a single 20 mm x 2 mm slit to scan the mirror in azimuthal direction, a diagonal slit with 1 mm section has been used to isolate the different part of the glasses in combination with the long slit to isolate the single layer. This procedure solves the alignment problems occurred with the PoC#4 [10] but can be further optimized due to the limited diagonal mask length and aperture. In fact, due to the limited azimuthal aperture the edges of the glass were not measured. Moreover, the width (1 mm) of the aperture was a bit too small for an efficient characterization procedure. In order to avoid

this kind of problems in the future, a new procedure with two slits (one fixed on the plate pair and the other orthogonal and displaced in vertical along the glass azimuth) is foreseen.

Due to the limited amount of time available, only two pencil beam scans were possible: the PP0 and the PP3 were selected. The PP0 data is useful for metrology comparison, while PP3 is the best layer of the PoC#5d. Furthermore, it represents the best achievement within the inner layers integrated so far, also considering the previous POCs. The measurement results available on the PoC#5d are reported in Figure 19. The images of the whole pencil beam scans have been created as composition of single pencil beam scans. For each pencil beam data, in the top panel it is shown the integrated intensity profile acquired (linear colour scale) while on the bottom panel is indicated the corresponding HEW value. On the pencil beam scan image we have marked (circles in magenta) the positions of the barycentre along the displaced direction.

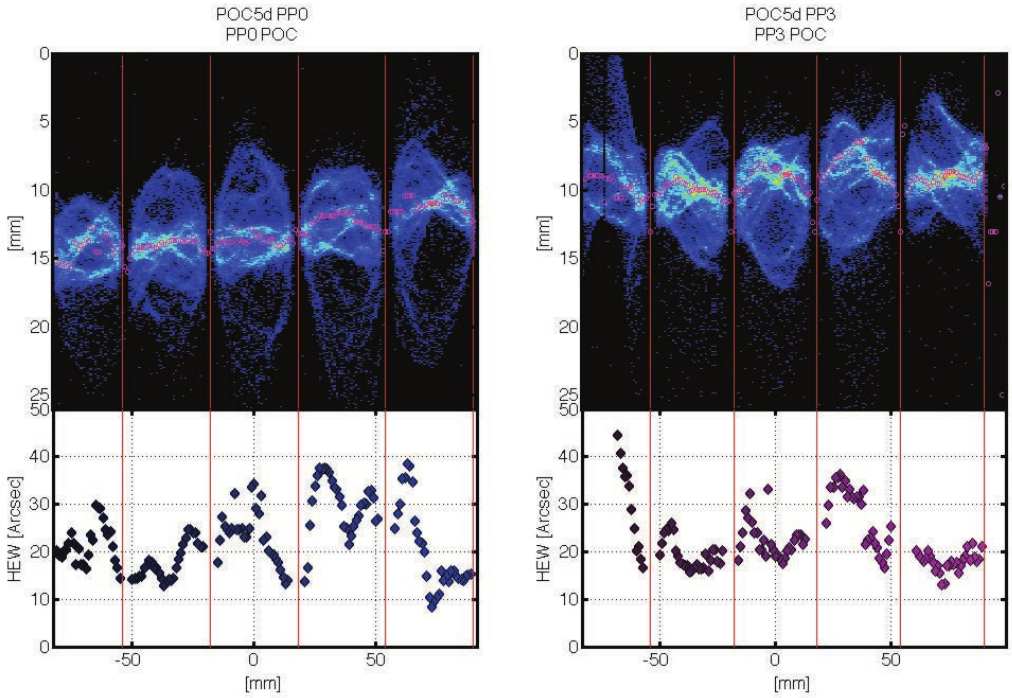

Figure 19: Pencil beam scans @1.49keV for PP0 and PP3 (PIXI data, Panter/MPE). On the top panels, the reconstructed images at the focus of the double reflected focal spot. On the bottom panels, the retrieved HEW values for each beam with intensity over the 60% threshold of the maximum intensity.

The HEW values corresponding to low intensity level have been removed in the graph: the selection has been performed calculating for each glass the maximum intensity along the different pencil beams and discarding the pencil beam data points with less than 60% intensity with respect to this value. The PIXI detector is not a real photon counter but 'relative' assessments can be performed with the same level of confidence of the HEW determination. In the top panel of Figure 20 the derived intensity value for each layer are shown, while on the bottom one the full set of HEW values is reported.

Additionally, an incorrect beam alignment can degrade further the HEW of the complete layer when the entire azimuthal aperture is considered. As observed with the PoC#4, the barycentre positions of the single pencil beam scans, reported in Figure 21, show an evident geometric effect, i.e. jumps of about 1mm appear in the 'transverse' position. There is a displacement of 3-4 mm along the 'longitudinal' direction for PP0 and a modulation of around 2 mm for PP3. The PP0 'transverse' jumps are in opposite direction with respect to the other layers, but also in opposite direction with respect to PoC#4. These results are quite similar to those observed during PoC#4 calibration, where a misalignment of around 80" around X-axis was conjectured and then measured. As the alignment settings are the same and the results are coherent, it is possible that some parts of the autocollimator optical chain (prisms and mirrors) have been damaged during the time. As some auxiliary parts of the alignment system (the capacitive sensors) have been dismounted from the BK7 integration molds for allowing their figuring (with ion beam), in the current situation it is not possible a complete verification on the system.

Furthermore, even when the ion beam figuring of the BK7 integration mold is completed, all the alignment procedure with 3D metrology has to be repeated and probably the setting will be different.

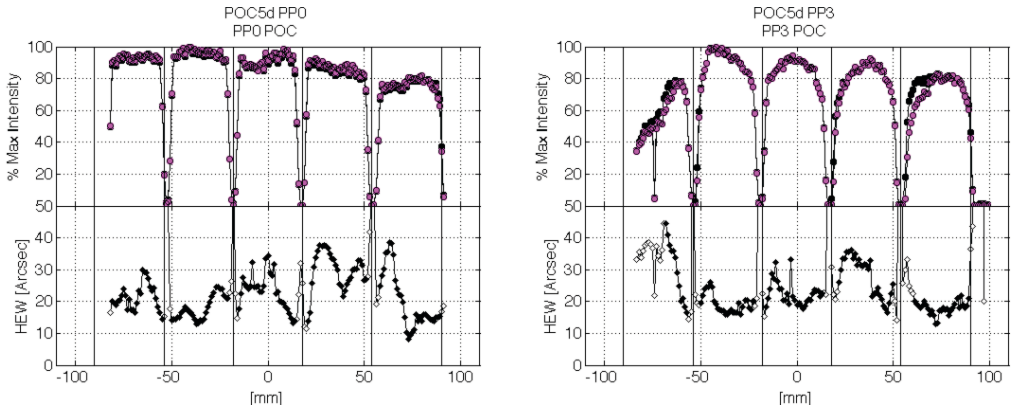

Figure 20: On the top panel, the percentage of the beam intensity with respect to the maximum one found in the same PP scan. On the bottom one, the corresponding HEW values: in black the data point for which the percentage is beyond 60%, in white the discarded ones.

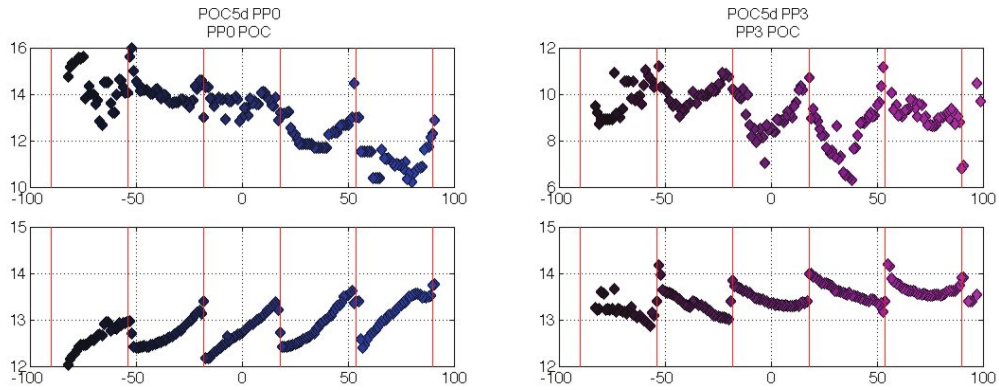

Figure 21: For each beam, on the top and on the bottom panels, the positions along the 'longitudinal' and 'transverse' direction of the beam spot barycenter as determined during the pencil beam scans.

As anticipated, the results for PP0 do not correlate with the expected performances derived from the metrological data available. Following the metrological results with respect to the glass micro-roughness, their contribution to the HEW should be almost negligible [9]. Therefore, the figure error of the glass should be the major driver for the result. Even taking into account the full 3d geometry derived from CUP map (which includes some azimuthal artefacts due to the carriages inaccuracy), the HEW, simulated in pencil beam, is well below the measured values (see figure 22, top right panel).

From a general point of view, it is possible to change the barycentre positions:

- the rotation around X-axis of the hyperbolic section with respect to the parabolic one introduce a tilt in the theoretical horizontal distribution along X-axis. In figure 22 (middle right panel), the tilt in the barycentre positions along the X-axis has been simulated assuming a misalignment of 80" (the same value derived from post-calibration metrology on PoC#4) around X-axis; the inferred barycentre trace is almost compatible with the measured one, even if the shape is not completely equal.
- the bumps in the Y-axis directions are introduced by azimuthal deformations on the plate surface. The measured amplitude of 1 mm is too high to fit the measured bumps (bottom right panel). In contrast, an amplitude of around 2.5 microns would be compatible with the measured displacements.

In order to respect the symmetry of the system and reduce the systematics in the measurement results, the figure error metrology is carried out on the CUP with the optical axis vertical. As the optical axis is horizontal during the x-ray calibrations, it would be appropriate to crosscheck the result in this condition, even if no major difference is expected from FEM simulations.

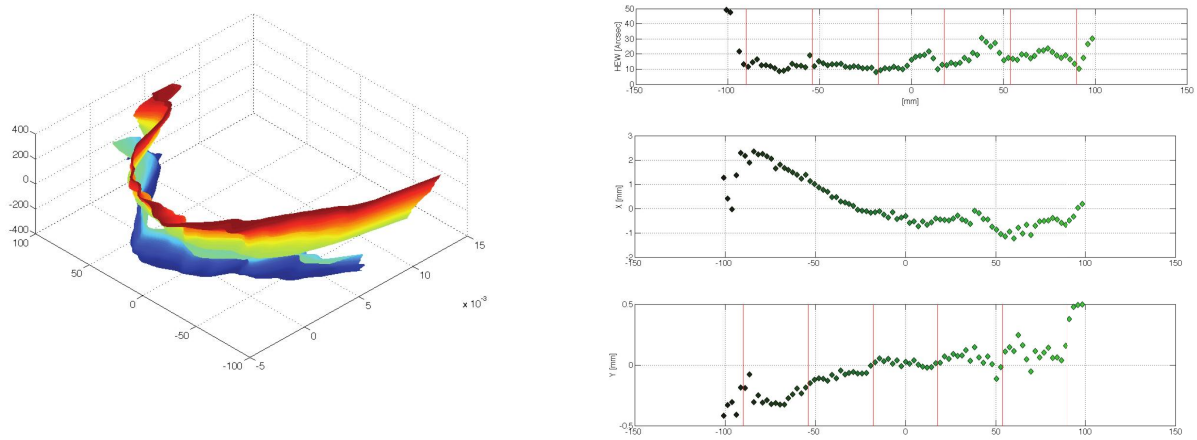

Figure 22: Ray-tracing results from CUP 3d Maps. (A) Residual figure error with respect to the Wolter-I configuration. (B) Simulated HEW, assuming an azimuthal pencil beam scan. (C) baricenter positions of the pencil beam data in X direction. (D) baricenter positions of the pencil beam data in Y direction.

5 Integration of thin glasses using Cold slumping

A first Willow Prototype (WP0) has been integrated in 2015. It was based on two out of the five Willow glasses (200 micron thickness) initially purchased by Corning. In order to reduce the realization costs, an aluminium backplane has been used as supporting structure, while BK7 ribs were used as interface. Owing to the differences between the CTEs of the materials, the thermal deformations are expected to contribute for some arcsec assuming a temperature control of +/-1°C. The metrological characterization of WP0 demonstrated that it was not correctly bonded on the lateral ribs. Nevertheless, the central part was compatible with an HEW of around 20" in single reflection [11]. In order to provide a more stable item to be transported and tested in Panter/MPE, the WP0 has been dismounted and another prototype fabricated.

5.1 Integrated prototypes: results and analysis

As the best glasses of the set were already used, two different glasses have been integrated. The figure error of the WillB and WillD glasses used to make the WP0 has to be compared with the one of the WillA and WillE glasses used for WP1. The shape errors are reported in Figure 23 using the same z scale. The quality of the plates integrated in WP1 was much lower than that of the plates for the WP0. In the first case the errors were of few hundreds of microns (PtV are in the range 160-180 microns), while in the second case are almost one thousand micron (PtV are in the range 660-930 microns).

The quality of the second module was really higher than the first one: the ribs were completely bonded up to the edges and the glue was well distributed all along the ribs without discontinuities. The measurements acquired with the CUP on the two sections of WP0 and WP1 are compared in figure 24. On the left the longitudinal residuals acquired on parabolic sections are shown, while on the right the hyperbolic sections are reported. For the WP1 the integrated glasses are well constrained all along the ribs profiles up to the azimuthal and the longitudinal edges. Moreover, no major deformations are present in correspondence of the ribs as it was in the case of WP0. In this case, in the positions where the thickness of the glue was not sufficient to keep the glass at a certain distance from the ribs, the glass shape is distorted.

The PtV and the RMS of the different longitudinal profiles are reported in figure 25. The data acquired on WP0 and WP1 are compared with the one acquired on POC3. This is an old module fabricated starting from hot slumped glass in cylindrical configuration. In this last case, the thickness was 400 microns and the longitudinal errors along the optical axis

were around 10 microns [14]. For the WP0, only the data of the central sections are reported, as the remaining part of the glass is not representative. Nevertheless, it is clearly visible that the bonding in correspondence of some of the ribs is not effective and this translates in higher amplitude of the adjacent errors. In the area between the ribs, the PtV and the RMS of the WP1 are almost doubled with respect to the WP0 values.

The corresponding HEW on the different longitudinal scans has been evaluated for parabolic and hyperbolic sections. The defects in the bonding of WP0 appear clearly as a local degradation of the HEW. Due to the local deformations, it is not possible to have a full correspondence between the original glass error and the integrated plate results. On one side, the PtV and the RMS for WP0 are almost halved with respect to WP1 where the glass is better constrained. On the other side, the HEW, as function of mid and long error frequency content, has not always the same behaviour.

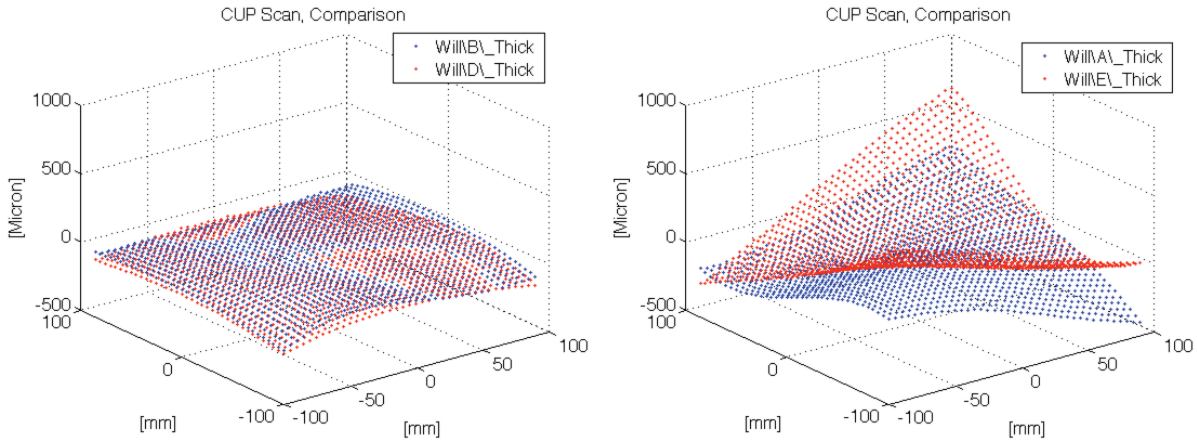

Figure 23: Initial flatness of the glasses used to build the WP0 and the WP1.

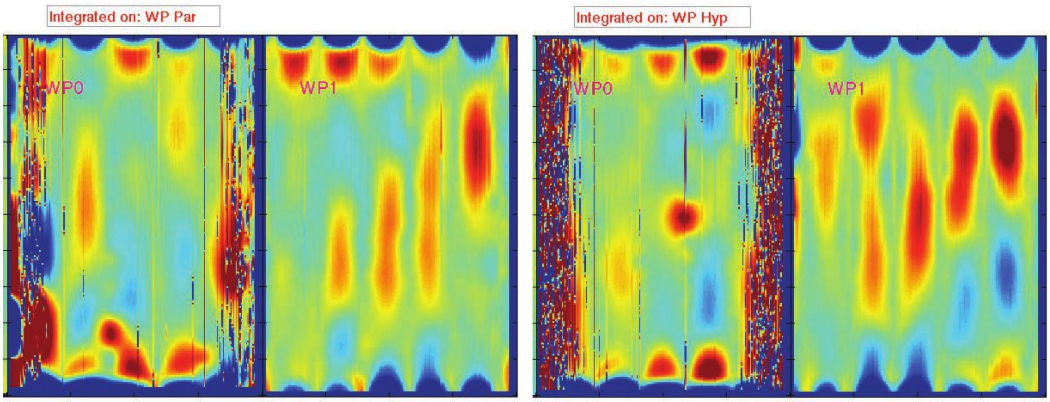

Figure 24: Parabolic and Hyperbolic sections of WP0 and WP1 integrated glasses as measured by CUP. Longitudinal detrend of the residual error is shown with a color scale of 4 microns PtV in all the cases.

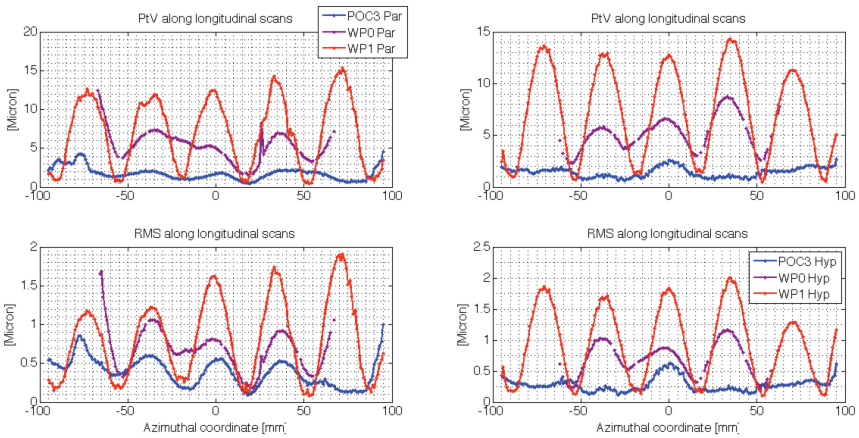

Figure 25: PtV and RMS of the longitudinal profiles of Parabolic and Hyperbolic sections of WP0 and WP1. For comparison, the POC3 data, realized with slumped glasses, are shown.

From a general point of view, besides for local distortions, the comparison shows that the low frequency errors dominate the HEW. As the measured amplitude of the low frequency errors is lower for the WP0 with respect to WP1, it follows that:

- The use of glasses characterized by lower figure error amplitude should guarantee better optical quality of the assembled optics.
- By choosing an appropriate ribs pattern, it is possible to improve the optical performances of the integrated glasses.

As in the case of the SGO, FEM simulations of the cold slumping process may starts from ad-hoc simulated error shapes or from the metrological data acquired with the CUP. Therefore, in order to have a better control on the expected results, we are currently working on the crosscheck of the metrological output with the FEM simulations. The results are still under analysis: the overall shape of the glass, with the bended edges, is similar, but they do not replicate completely the measured pattern of the spring back effect. Further analysis will be carried out for a better prediction for the experimental results.

5.2 WP1 X-ray calibration results

The WP1 module has been measured in full illumination and in pencil beam at Panter/MPE [13] end of June 2016. The available data (full illumination @1.49keV) are reported in figure 26A. Despite the very poor initial quality of the thin glasses, the measured HEW @1.49keV is 49.1", still comparable to the one achieved so far with the SGO based on hot-slumped glass technology by our group.

Being definitively below one arc minute, the measured HEW is already compatible with experiments in which the optical performances are a little relaxed in favour of the effective area, such as the Chinese X-ray Timing and Polarization mission (XTP) [26]. The mission includes a High energy X-ray Focusing Array (HFA), a Low energy X-ray Focusing Array (LFA), a High energy X-ray Collimated Array (HCA) and Wide Field Camera. The HFA with a focal length of 5.5 m is located in the middle of the satellite platform. The X-ray optics is a quasi-Wolter-I type, focusing x-rays in the range of 1–30 keV with an angular resolution of about 1 arc minute and a field of view of 16 arc minutes.

Moreover, this is a really encouraging result, as improvements in the optical performances are easily expected:

- starting from better quality glasses;
- matching better the CTE of the backplane (in aluminum for the WP1) and of the ribs (in BK7 for the WP1) with the one of the Willow glass.

With respect to the x-ray calibration data, the image appears quite broad in azimuthal direction (2 mm) and the edges effects extend the focal spot in all directions. The azimuthal size of the spot is affected by the azimuthal pattern of the glass. Using

the 3d maps provided by the CUP (see figure 26B), it is possible to reproduce partially this feature of the focal spot (figure 26C). Additional azimuthal aperture may also be introduced by the misalignment of the plates around X-axis, as observed for PoC#4 [10] and inferred for PoC#5d (see paragraph 4.4). A clear and complete view of the behaviour of the system will be possible when the all data for the pencil beam scan performed on the WP1 will be available. In any case, the impact of the azimuthal error is almost negligible when covered by the longitudinal profiles errors. Instead, assuming perfect longitudinal profiles conditions, it increases almost linearly the HEW, scaling around 1.3" for 1micron PtV error.

Due to operational constrains, in general the shape error is mapped up to around 5 mm from the edge of the glass. This corresponds to the 10% of the glass area lost, exactly in the positions where the edge effects are higher. It will be necessary to increase the measurement area in order to fully reproduce the behaviour of the focal spot: with the current metrological data, the expected HEW (33") is in fact lower than the measured one.

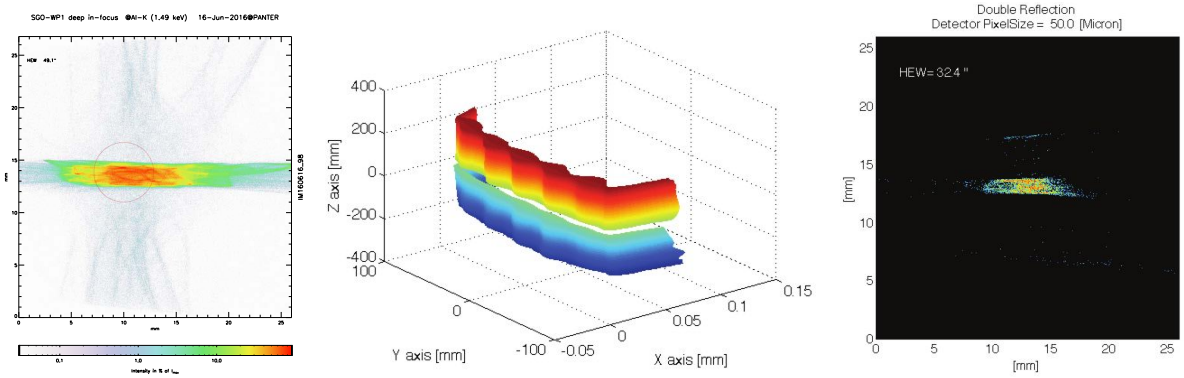

Figure 26: WP1 Full illumination, data acquired @1.49keV with PIXI at Panter/MPE. (B) Azimuthal pattern measured with CUP on the hyperbolic section of the module. The PtV of the error depends on the azimuthal position and ranges between 2 and 7 microns of amplitude. (C) Example of the focal spot expected from the 3d error map.

5.3 Future development

As the initial tests were performed with a limited amount of samples, in order to continue with the cold slumping activities new sets of glasses have been procured. Two stocks of 50 glasses with thickness of 100 micron and 200 microns have been purchased from Corning. These new Willow glasses are square, 200 mm x 200 mm. The set with a thickness of 200 microns has been characterized in terms of figure error and thickness variations. The measures have been carried out with the CUP [19] using the CHR sensor in thickness mode and deriving the figure error from the front surface data. The glasses were placed in vertical condition supported by two points on the bottom and with one on the top back. This configuration is expected to introduce low frequency errors in the glass due to the gravity distortion. Nevertheless, the deformations are expected on the order of few microns and therefore negligible in comparison with intrinsic shape error. The results achieved on the sample are reported in figure 27. For each glass the error map is shown in microns.

The glasses are affected by low frequency errors in longitudinal and azimuthal directions. The corresponding PtV in the overall map, considering just the longitudinal direction, is reported in figure 28A in red and in blue. In figure 28B it is reported the error range distribution. Most of glasses have an overall error with PtV around 100 microns, with around 50 microns error in longitudinal direction. The thickness variations are almost all in the range 1-2.5 microns, but with a preferential direction.

With respect to the out-of-flatness, this new set of glasses is better compared to the first samples procured in 2015. The mean overall PtV of their figure error is even smaller than the one of the WillB and WillD sample used to realise the WP0. A detailed FEM simulation activity is being carried out to predict the expected results in dependence of the shape of the initial out-of-flatness. FEM preliminary results indicate that the first harmonics on the shape error can be corrected almost completely (final HEW of few arc seconds), as soon as their amplitude is less than 100microns. Their experimental validation will be performed with the realization of new prototypes in the next months.

The new glasses will be used in the future to prove the cold slumping process in at least two different optical configurations. The activity on the BK7 moulds (20m focal length and 1m radius of curvature) will be continued; nevertheless, due to the actual integration mould configuration (the references for the alignment setting have been dismounted), the layers could be evaluated in single but not in double reflection. In any case, the results will be compared with the one obtained with FEM simulations in order to improve their predictive capability. Other integration moulds in aluminium are available (8.4 m focal length and 0.485 m radius of curvature). The comparison between the results achieved in the two different configurations will guarantee a robust validation of the FEM model.

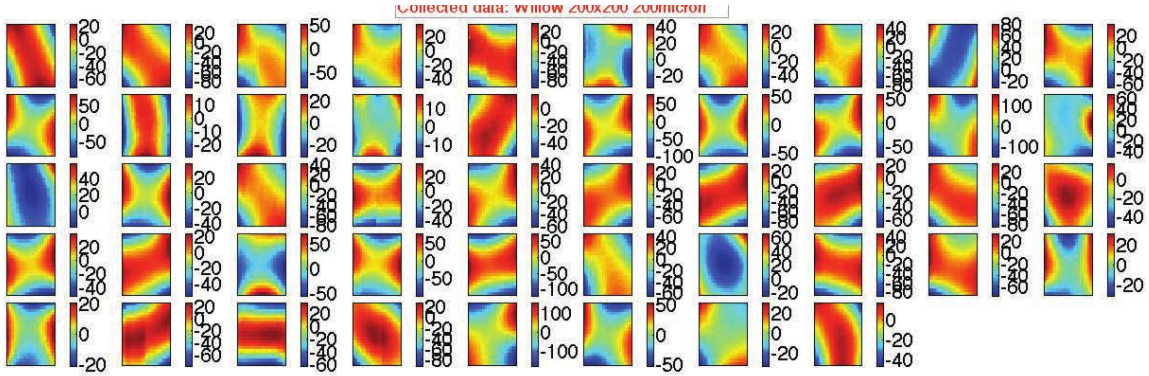

Figure 27: Residual error map with respect to a flat of the different samples (Willow glasses, 200 mm x 200 mm, 200 microns thick). In each panel, the color scale is in microns.

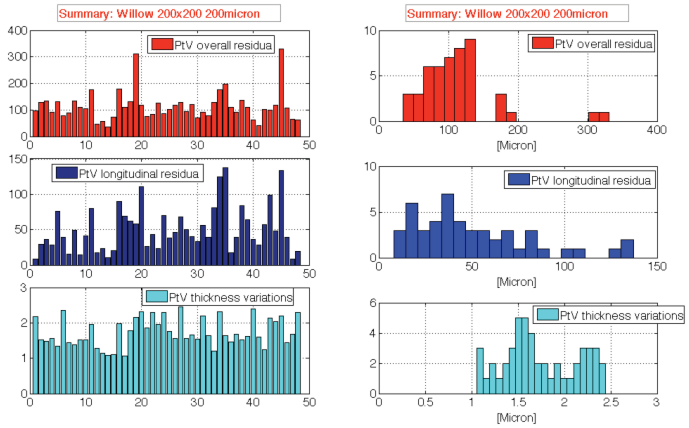

Figure 28: (A) The overall PtV of the flatness error of the different glass sample. (B) The longitudinal PtV of the flatness error of the different glass samples. (C) The PtV of the thickness variation maps.

6 Conclusions

We have presented an update of the integration activities and of the recent up-grade of the IMA. The introduction of the dust particle detection system based on the deflectometry has been very effective and fruitful. The system enables the characterization of the level of cleanliness reached following different cleaning procedures. Therefore, the comparison of the results allowed us to select of the most efficient one. In the current situation, we have observed that an improvement in the optical paper quality was a major advance during the set-up of the glass. A nice correlation (in correspondence of the ribs) has been found between the dust grain (entrapped between the moulds and the optical surface of the glass during the preparatory phase) and the resulting deformation on the shape of the glass after the integration. The metrology possibilities on board of the IMA will be further extended: a deflectometric system for the characterization of the integrated plates in the stack is currently under development and will be operative in the next months. Moreover, the glue distribution system has been recently improved in order to guarantee a better control on the amount and on the positioning of the glue. The new

procedure allows a complete bonding of the ribs up to the edges: this is fundamental for the cold slumping approach as it reduces to the minimum the edge effects.
At the moment, the hot-slumping activities in INAF/OAB are in stand-by and no new slumped glasses are in production. The last available slumped glasses have been integrated in the PoC#5 beginning of 2016. The x-ray calibration results obtained in June 2016 are not fully in agreement with the available metrological data. The HEW @1.49keV of the different PPs (around 30") is not better than the one achieved with older prototypes. Further metrological campaign will be carried out to explain the mismatch. Nevertheless, improvements in the bonding have been observed in the calibration results: the area near the ribs is of better quality with respect to the rest of the glass. The results achieved on the POC#5d do not demonstrate a real limit for the technology: a fundamental improvement is related to the level of cleanliness reached during the glass-positioning phase. This is the main operational aspect that requires a refinement. An efficient solution could be the introduction of an additional clean tent (of ISO4-ISO5 class) to cover the moulds area during the preparatory phase.
A new prototype based on first generation Willow glass has been produced and measured in full illumination at Panter/MPE with a final HEW of 49.1". As this prototype was built starting from very poor quality flat glasses (PtV of the error of the order to 600-900 microns), this is an excellent result. Moreover it is very promising, as the characterization of the set of glass available for the next activities shows that they are improving the out-of-flatness. Preliminary FEM simulations show that the magnitude and the low frequency shape of their figure errors are compatible with an effective cold slumping replica. Further activities related to the improvement of the FEM predictive capabilities and to the comparison with the integrated item results will be the basis of the working program.
From the analysis of the available molds and the possible optical configurations it follows that in the near future the integration activities will concentrate on shorter focal lengths and smaller radii. This has the advantage of a simpler set-up for x-ray calibration. As drawback, the metrology on this kind of optics is more difficult with the available CUP set-up. The same configuration will be used for testing the hot-slumped glass provided by NASA and for investigating the cold shaping approach with flat Willow glasses.

Acknowledgments

This research is supported by ASI (the Italian Space Agency).

References

(1) M. Bavdaz, N. Rando, E. Wille, K. Wallace, B. Shortt, M. Collon, C. van Baren, G. Pareschi, F. Christensen, M. Krumrey, M. Freyberg, "ESA-led ATHENA/IXO Optics Development Status", SPIE 8147, 81470C (2011).
(2) M. J. Collon; S. Kraft; R. Günther; E. Maddox; M. Beijersbergen; M. Bavdaz; D. Lumb; K. Wallace; M. Krumrey; L. Cibik; M. Freyberg, "Performance characterization of silicon pore optics", Proc. SPIE 6266 (2006)
(3) W. W. Zhang, M. P. Biskach, V. T. Bly, et al., "Affordable and lightweight high-resolution x-ray optics for astronomical missions," Proceedings of SPIE Vol. 9144, 914415 (2014)
(4) M. Ghigo, S. Basso, R. Canestrari, P. Conconi, O. Citterio, M. M. Civitani, E. Dell'Orto, D. Gallieni, G. Pareschi, G. Parodi, L. Proserpio, D. Spiga, "Hot slumping glass technology and integration process to manufacture a grazing incidence scaled prototype for the IXO telescope modules", Proc. SPIE 7437 (2009)
(5) M. M. Civitani, S. Basso, O. Citterio, P. Conconi, D. Gallieni, M. Ghigo, G. Pareschi, L. Proserpio, B. Salmaso, G. Sironi, D. Spiga, G. Tagliaferri, A. Zambra, F. Martelli, G. Parodi, P. Fumi, M. Tintori, D. Gallieni, M. Bavdaz, E. Wille, "Accurate integration of segmented x-ray optics using interfacing ribs", Opt. Eng. 52(9), 091809 (2013)
(6) M. M. Civitani, S. Basso, M. Bavdaz, O. Citterio, P. Conconi, D. Gallieni, Ghigo, M., B. Guldimann, F. Martelli, G. Pagano, G. Pareschi, G. Parodi, L. Proserpio, B. Salmaso, D. Spiga, G. Tagliaferri, M. Tintori, E. Wille, A. Zambra, "An integration machine for the assembly of the x-ray optic units based on thin slumped glass foils for the IXO mission," Proc. SPIE 8147, 81470R (2011)
(7) G. Parodi, F. Martelli, S. Basso, M. Bavdaz, O. Citterio, M. M. Civitani, P. Conconi, M. Ghigo, G. Pareschi, L. Proserpio, D. Spiga, E. Wille, A. Zambra, "Design of the IXO optics based on thin glass plates connected by reinforcing ribs", Proc. SPIE 8147 (2011)
(8) S. Basso, M. M. Civitani, G. Pareschi, E. Buratti, J. Eder, P. Friedrich, M. Fürmetz, "A design study of mirror modules and an assembly based on the slumped glass for an Athena-like optics", Proc SPIE 9603 (2015)
(9) B. Salmaso, S. Basso, M. M. Civitani, M. Ghigo, J. Holyszko, D. Spiga, G. Vecchi, G. Pareschi, "Slumped glass

optics development with pressure assistance", Proc. SPIE 9905, (2016)
(10) M. Civitani, S. Basso, C.Brizzolari, M. Ghigo, G. Pareschi, B. Salmaso, D. Spiga, G.Vecchi, E.Breuning, V. Burwitz, G. D. Hartner, B. Menz, "Slumped glass optics with interfacing ribs for high angular resolution x-ray astronomy: a progress report", Proc. SPIE 9603 (2015)
(11) M.M. Civitani, S. Basso, O. Citterio, M. Ghigo, B. Salmaso, G. Pareschi, G. Vecchi , " Cold shaping of thin glass foils: a fast and cost-effective solution for making light-weight astronomical x-ray optics ", Proc. SPIE 9603 (2015)
(12) S.Basso, M.M.Civitani, G.Pareschi, "Design of a medium size x-ray mirror module based on thin glass foils", Proc. SPIE 9905 (2016)
(13) V. Burwitz, M. Bavdaz, G. Pareschi, M. Collon, W. Burkert, M. D. Ackermann, G. Hartner, D. Spiga, M. M. Civitani, B. Menz, "In focus measurements of IXO type optics using the new PANTER x-ray test facility extension," Proc SPIE 88611J (2013)
(14) M. Civitani, M. Ghigo, S. Basso, L. Proserpio, D. Spiga, B. Salmaso, G. Pareschi, G. Tagliaferri, V. Burwitz, G. D. Hartner, B. Menz, M. Bavdaz, E. Wille, "Direct hot slumping and accurate integration process to manufacture prototypal X-ray Optical Units made of glass," Proc. of SPIE Vol. 8861, 886110 (2013)
(15) M. M. Civitani, M. Ghigo, G. Pareschi, B. Salmaso, D. Spiga, G. Tagliaferri, G. Vecchi, V. Burwitz, G. D. Hartner, B. Menz, " X-ray optical units made of glass: achievements and perspectives," Proc. SPIE 9144, 914416 (2014)
(16) L. Proserpio, E. Breunig, P. Friedrich, A.Winter, C. Rohé, J. Eder, V. Burwitz, G. D. Hartner, B. Menz, M. M. Civitani, S. Basso, E. Buratti, "JIM: a joint integrated module of glass x-ray optics for astronomical telescope," Proc. SPIE 9603 (2015)
(17) Zhang, W.W., et al., "Next generation astronomical x-ray optics: high angular resolution, light weight, and low production cost, " SPIE 8443, 88430S (2012)
(18) E. Breunig et al.," Characterising x-ray mirror deformations with a phase measuring deflectometry system," Proc. SPIE 9144 (2014)
(19) M. M. Civitani, M. Ghigo, O. Citterio, P. Conconi, D. Spiga, G. Pareschi, L. Proserpio, "3D characterization of thin glass x-ray mirrors via optical profilometry," Proc. SPIE 7803, 78030L (2010)
(20) B. Menz, V. Burwitz, G. D. Hartner "Measuring SPOs at the PANTER x-ray test facility: the alignment", Proc. SPIE 9905 (2016)
(21) Zhanshan Wang et al. , "Development of the X-ray Timing and Polarization telescope optics", Proc SPIE 9144, 91441E (2014)